IEEE Access
Multidisciplinary ⋮ Rapid Review ⋮ Open Access Journal

Received January 6, 2022, accepted January 20, 2022, date of publication January 27, 2022, date of current version February 4, 2022.

Digital Object Identifier 10.1109/ACCESS.2022.3147217

Material Permittivity Estimation Using Analytic Peak Ratio of Air-Coupled GPR Signatures

BUDIMAN P. A. ROHMAN[1,2], (Member, IEEE), MASAHIKO NISHIMOTO[1], (Member, IEEE), AND KOHICHI OGATA[1], (Member, IEEE)

[1]Faculty of Advanced Science and Technology, Kumamoto University, Kumamoto 860-8555, Japan
[2]Research Center for Electronics and Telecommunication, National Research and Innovation Agency, Bandung 40135, Indonesia

Corresponding author: Budiman P. A. Rohman (budi057@brin.go.id)

ABSTRACT Ground penetrating radar (GPR) is widely applied for civil engineering, such as for building health assessments or pavement inspections. In these applications, information on the material permittivity is important for internal structure inspection and characterization. However, in the case of a large building area, a lightweight, fast and effective permittivity measurement technique is required. In addition, the estimation method for different GPR types and range configurations must be generalized for adaptability and wide applicability. This paper proposes a material permittivity estimation technique for air-coupled GPR that effectively works for mobile and large observation missions. The method employs the peak ratio of analytic representation signals between the antenna direct coupling and the material surface reflection. An interpolation algorithm is applied to the reference characteristic curves generated by the finite-difference time-domain technique to adapt the change in radar range configuration. The proposed method has been tested to estimate the permittivity in three different construction materials and measure two metal rebar depths inside reinforced concrete. The experimental results show that the method works with acceptable accuracy. Therefore, the method is sufficiently promising to be utilized in real applications, especially those that require adaptability and mobility, such as ground and aerial vehicle-based radar systems.

INDEX TERMS Permittivity estimation, ground-penetrating radar, radar signal processing, analytic signal.

I. INTRODUCTION

Ground penetrating radar (GPR) is a mature nondestructive testing and evaluation technology that is mostly used to explore the subsurface of objects [1]. Currently, this radar is also applied to inspect buildings and structural health [2]. Some studies on these cases have reported promising results in several specific applications such as rebar detection [3], [4], void detection and parameterization [5], defect detection [6], and rebar corrosion state estimation [7]–[9]. Researchers mostly employ internal imaging from GPR B-scan data to assess the building's health. However, to accurately characterize this image, information on material permittivity is a crucial need. In addition, since the building area will be very large and may have spatially different permittivity values, an effective and accurate permittivity estimation method is required.

Various material permittivity estimation methods have been proposed that appear promising in their application. However, most of those techniques are based on the time domain or frequency domain analysis of the surface propagation waves that are detected by ground-coupled type GPRs [10]–[14]. Since both transmitting and receiving antennas of ground-coupled GPR are in contact with the material [15], it takes considerable time for a point-by-point measurement; thus, their application is limited to relatively small areas. To inspect a very large area with high spatial resolution, the use of air-coupled GPRs is more promising than the ground-coupled type, since they can be mounted on mobile platforms and measure faster [2], [15] (see Fig. 1). This air-coupled technique widely opens the possibility of measurement by employing unmanned vehicle systems such as drones or ground-based robots for an effective mission, as discussed in [16]–[18]. Air-coupled GPR has been studied for soil moisture estimation using the amplitude of surface reflected waves [19], [20]. Nevertheless, this technique requires accurate calibration and has the limitation of being sensitive to the

The associate editor coordinating the review of this manuscript and approving it for publication was Chengpeng Hao.

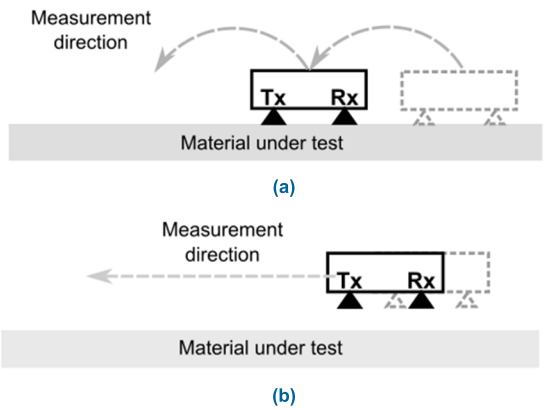

FIGURE 1. Comparison of measurement process by using: (a) ground-coupled, and (b) air-coupled GPR.

input waveform and antenna configuration. Widely accepted methods such as those in [21], which use the reflection ratio between the material under test and a perfect electric conductor, are also possible in this case. However, this measurement requires a constant distance between the antenna and the material to synchronize with the amplitude of reference. The proposed methods in [22], [23] are complicated and require a relatively complex computation. A common midpoint-based method was proposed in [24], [25], but those methods require multiple antenna/radar or multiple ranges of measurements, which makes application complicated. Another estimation that applies to the GPR of this type was proposed in [26], [27]. The proposed method can estimate the permittivity with high accuracy, but it requires a large computation time for full-wave inversion.

According to this background, this paper proposes a new and relatively efficient signal processing technique to estimate the material permittivity in air-coupled radar systems. As a feature, the method employs the peak ratio of the analytic signal representation between material surface reflection and direct antenna coupling. A simple look-up table and interpolation techniques are applied in the final estimation step using a finite-difference time-domain (FDTD)-based characteristic curve as a reference. The use of analytic signal representation of radar signature, antenna coupling signal, and FDTD-based plot as a base of estimation is an innovative approach of this proposed method, which has not been proposed or used by existing methods based on our knowledge. In addition to the simplicity and accuracy, the proposed method aims at fast, remote, nondestructive mapping for most types of GPRs and configurations. Furthermore, by the generality of the method against difference waveforms and center frequencies, the method can be implemented in applications employing future cognitive radar techniques that must change the parameters during the measurement [28], [29]. The adaptability of the method against the change in range between antenna and material also enables the method to be implemented on unmanned ground-based or aerial-based GPR systems, which are commonly unstable because of many factors.

Some preliminary results of the investigation of this method have been performed and presented in [30], and this manuscript deeply extends the analysis to verify the method through controlled laboratory experiments. The results of this study comprehensively demonstrate the feasibility of the implementation of this method in real applications.

The remainder of this paper is organized as follows. In section II, the basis of material permittivity estimation and the proposed method is briefly explained, followed by the numerical simulation and experimental setup description in section III. The results and discussion regarding this study are explained in section IV. Finally, the conclusion of this study is described in Section V.

II. ESTIMATION OF MATERIAL PERMITTIVITY

For the internal imaging of concrete using B-scan data measured by GPR, the electrical properties of the concrete, i.e., permittivity ε and conductivity σ, must be accurately estimated for high-resolution imaging. The electrical conductivity represents the current density that results from an external electric field, while permittivity is a complex-valued property that represents the level of a medium's ability to be polarized from other external electric fields. The complex permittivity ε_c is defined in terms of ε and σ as

$$\varepsilon_c = \varepsilon - j\frac{\sigma}{\omega} = \varepsilon^{'} - j\varepsilon^{''} \tag{1}$$

where the real part $\varepsilon' = \varepsilon$ is the dielectric constant, and the imaginary part $\varepsilon^{''} = \sigma/\omega$ is the loss factor that represents energy loss because of absorption. The dielectric constant is commonly represented by the relative permittivity ε_r, which is found by dividing by the free space permittivity $\varepsilon_0 = 8.854 \times 10^{-12} F/m$. This dielectric constant will change mostly due to its water content and high loss factor [19]. Since the reflected wave is distorted in relation to the medium permittivity, we estimate these parameter values using the reflected wave.

The proposed method consists of four main steps, as illustrated in Fig. 2. The first step is the preprocessing of the recorded radar signal containing direct-current removal and bandpass filter. The second step is the computation of analytic signal which is then the ratio of the peak of analytic signal between antenna coupling with surface reflection is computed. Third, the result is used to calculate the analytic peak ratio using a pre-determined shift factor constant. Finally, the material permittivity is estimated by interpolating the analytic peak ratio using a characteristic curve made by the FDTD method. The detail of the step is described as follows.

A. PEAK RATIO OF ANALYTIC SIGNAL

The analytic signal of the GPR response A_s is expressed by using the Hilbert transform pair as follows:

$$A_s(t) = x(t) + iH\{x(t)\} \tag{2}$$

where

$$Hx(t)\} = \frac{1}{\pi} P.V. \int_{-\infty}^{\infty} \frac{x(\tau)}{\tau - t} d\tau \tag{3}$$

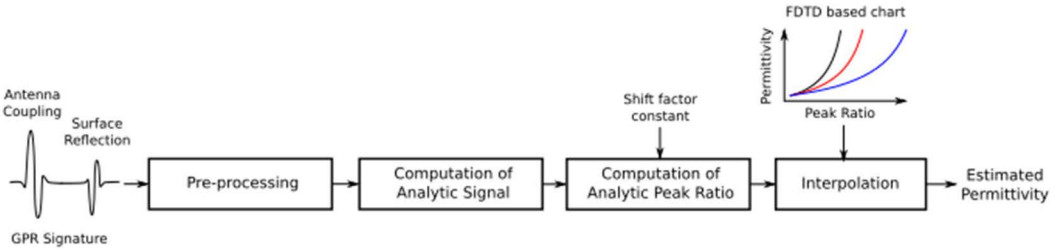

FIGURE 2. Proposed signal processing technique.

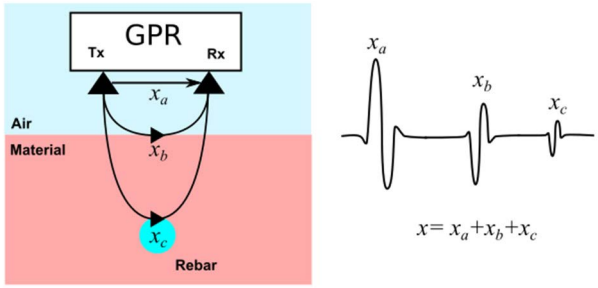

FIGURE 3. The component of air-coupled GPR signature.

where $x(t)$ is the GPR response, $i = \sqrt{-1}$, $Hx(t)\}$ is the Hilbert transform, and P.V. is the Cauchy principal value. This study focuses on air-coupled GPR because this type is more applicable for high mobility and large observation missions. Additionally, for this radar type, the direct antenna coupling signal can be a reliable reference for the estimation calculation. Commonly, this signal will be removed, but in this study, it will be greatly employed. As shown in Fig. 3, the air-coupled GPR signal consists of three components, including direct antenna coupling x_a, material surface reflection x_b, and embedded object reflection x_c, which is expressed as:

$$x(t) = x_a(t) + x_b(t) + x_c\,(t) \tag{4}$$

The material surface reflection is the signal reflected from the object's surface to the receiver. This signal correlates with the reflectivity of the material, which has a close relationship with the permittivity value. The reflectivity from material 1 to 2, Γ, is defined as:

$$\Gamma = \frac{\sqrt{\varepsilon}_1 - \sqrt{\varepsilon}_2}{\sqrt{\varepsilon}_1 + \sqrt{\varepsilon}_2} \tag{5}$$

where ε_1 and ε_2 are the dielectric constants of material 1 and material 2, respectively. In the case of air-coupled GPR, in the first reflection, material 1 is defined as air, so that the reflectivity to material 2 can be written as:

$$\Gamma = \frac{1 - \sqrt{\varepsilon}_2}{1 + \sqrt{\varepsilon}_2} \tag{6}$$

Therefore, intuitively, the material surface reflection contains information on the permittivity of material 2. Since the direct antenna coupling signal is constant and can be a good reference for the generalization of the estimation method, this study elects to use this signal. The proposed feature is called an analytic signal peak ratio (Δ_p), which is mathematically defined as:

$$\Delta_p = \left|\frac{p_g}{p_c}\right| + F \tag{7}$$

with

$$F = \Delta_{p,e} - \Delta_{p,s} \tag{8}$$

where p_g and p_c are the peaks of the analytic signal of material surface reflection and direct antenna coupling, respectively; F is the shift factor; $\Delta_{p,e}$ is the peak ratio of experimental data of a known material; $\Delta_{p,s}$ is the peak ratio of simulated data with a similar permittivity to a corresponding known material. The shift factor F is required to relate the radar type and configuration ratio in the experiment with the FDTD simulation-based characteristic curve. This value will shift the obtained analytic peak ratio from the experimental data to conform to the simulation reference curve. Some differences in the GPR configuration, such as antenna design and type, will be compensated by employing this constant.

B. INTERPOLATION TECHNIQUE

In an air-coupled GPR, both antenna–material and transmitting-receiving antenna distances can be configured by various means. We use the GPR configuration ratio x/y to name both distances established. For example, a configuration ratio of 4/5 (8/10) indicates that the antenna-material distance is 4 cm and the transmitting-receiving antenna's distance is 5 cm. Seeing a change in correlation between permittivity and the proposed feature depends on the GPR configuration ratio, to conduct an estimation with experimental data, we simply apply the linear interpolation method to the recorded correlation function with several GPR configurations.

Simple linear interpolation is used to estimate the permittivity target material $\tilde{\varepsilon}_r$ with peak ratio Δ_p, as shown by the equation below (see Fig. 4):

$$\begin{aligned}\tilde{\varepsilon}_r &= I\left(\Delta_p, \Delta_{p1}, \Delta_{p2}, \varepsilon_{r1}, \varepsilon_{r2}\right) \\ &= \varepsilon_{r1} + (\Delta_p - \Delta_{p1})\frac{(\varepsilon_{r2} - \varepsilon_{r1})}{(\Delta_{p2} - \Delta_{p1})}\end{aligned} \tag{9}$$

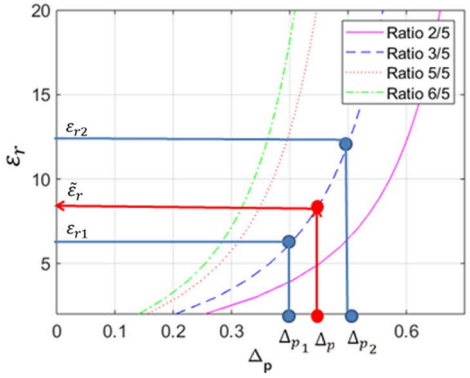

FIGURE 4. Interpolation using simulation data as a reference. As an example, the configuration ratio of experimental data is 3/5.

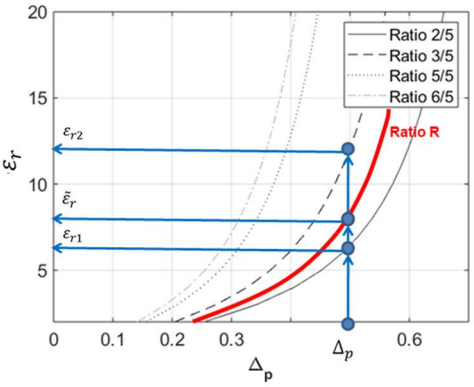

FIGURE 5. Interpolation using simulation data as a reference. As an example, the GPR configuration ratio of experimental data is between 2/5 and 3/5.

where Δ_{p1}, Δ_{p2}, ε_{r1}, and ε_{r2} are the neighboring simulated data of the peak ratio and relative permittivity, respectively. The peak ratio of both data flanks the peak ratio of unknown material.

If the GPR configuration is not presented in the recorded simulation data, we must apply a two-step interpolation method. The first interpolation is required to make a new correlation function, as follows (see Fig. 5): for each peak ratio value, we calculate the new characteristic curve for configuration ratio R. Assuming that the R-value is placed between ratio 3/5 and 5/5, or R_1 and R_2, respectively, the permittivity of peak ratio Δ_p is:

$$\tilde{\varepsilon}_{r,\Delta_p} = I\,(R, R_1, R_2, \varepsilon_{r1}, \varepsilon_{r2}) = \varepsilon_{r1} + (R - R_1)\frac{(\varepsilon_{r2} - \varepsilon_{r1})}{(R_2 - R_1)} \tag{10}$$

After we obtain the new curve with ratio R, a second interpolation is similarly applied to interpolation as Eq. 9 to find the targeted material permittivity.

C. GROUND TRUTH COMPUTATION

To test the method, we must know the ground truth of the permittivity of every testing material. Since the thickness of the material under test is known, the permittivity through the radar signal propagation time between front and back surface reflection was measured as follows (see Fig. 6 (a)). After the peak of the waveform was computed, the delay of wave reflection from the front and back surface reflections was calculated. Using the information of the material thickness and propagation time, the material relative permittivity can be approximated using the following equation:

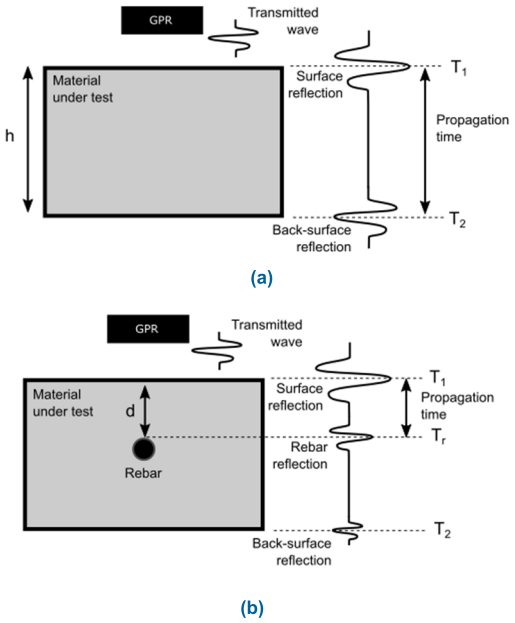

FIGURE 6. Delay time estimation for ground truth of: (a) material permittivity, and (b) reinforced concrete rebar depth.

$$h = \frac{c(T_2 - T_1)}{2\sqrt{\varepsilon_r}} \tag{11}$$

where h is the material thickness; T_1 and T_2 are the reflection times of the front and back surfaces, respectively; c is the electromagnetic wave velocity constant 3×10^8 m/s. This method is also used to estimate the rebar depth in the experimental study of the reinforced concrete in section IV. C, as illustrated in Fig. 6(b), where T_r and d are the reflection time and depth of the rebar, respectively (Eq. 12).

$$d = \frac{c(T_r - T_1)}{2\sqrt{\varepsilon_r}} \tag{12}$$

III. SIMULATION AND EXPERIMENTAL SETUP

To determine the relationship between analytic peak ratio and material permittivity, we employed synthetic data generated by FDTD-based software for an electromagnetic propagation model, gprMax [31]. A simple flat homogeneous box was used as the material model; the dielectric constant was 2-20, and the conductivity was 0.001-0.1 S/m. For the input pulse waveform, we used a monocycle pulse with a center frequency of 1-5 GHz. The GPR system employed a theoretical Hertzian dipole antenna. This antenna was selected because of the simple design and built-in availability in the software.

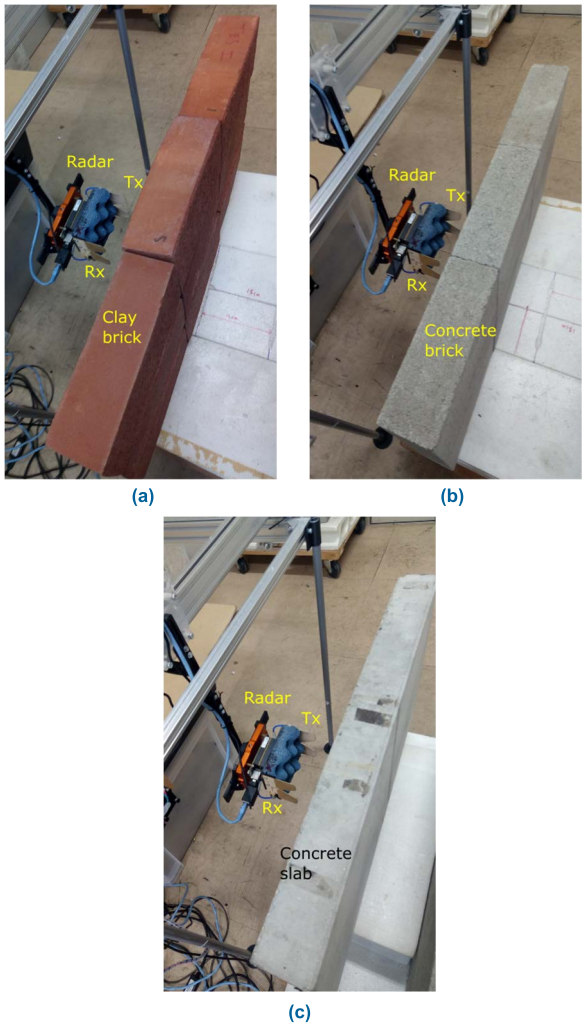

FIGURE 7. Experimental setup using ultra-wideband impulse radar for three materials: (a) clay brick, (b) concrete brick, and (c) concrete slab.

In addition, in this method, we focus on the use the waveform amplitude information regardless the antenna design and type. Of course, the difference in design of the antenna between this simulation and the real measurement will affect the correlation, but in this study, we consider employing the shift factor constant (see Eqs. 7 and 8). This constant aims to anticipate some configuration differences that cannot be avoided in the real measurement from the simulation due to the availability of a certain antenna.

In the experimental study, we used an ultra-wideband impulse radar module from Xethru with a frequency bandwidth of 1.5-6.0 GHz, the impulse waveform was a monocycle pulse, and the antenna was Bowtie. The number of samples recorded by the radar was 512 samples with frequency sampling of 39 Giga samples per second. The tested materials consisted of clay brick, concrete brick, and concrete slab. The measurement was taken at the center of the material. The range between radar and antenna was selected considering the evaluation of the effect of a configuration

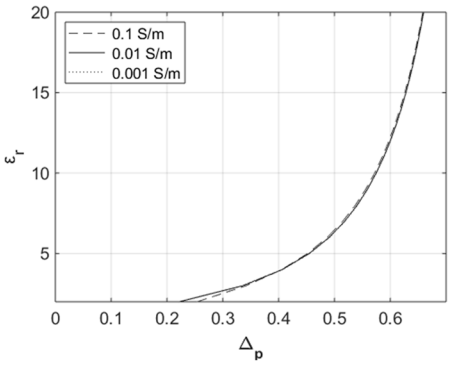

FIGURE 8. Effect of material conductivity to permittivity-analytic peak ratio relationship.

ratio setting. The range of transmitter-receiver antennas was fixed at 10 cm, while the evaluated configuration ratio was 6/10 to 10/10 (or 3/5 to 5/5). The radar was moved by the actuator. The experimental setup is shown in Fig. 7.

The recorded GPR response was pre-processed to extract the direct antenna coupling and material surface reflection signals. Those signals were transformed by Hilbert to compute the analytic signals. Both analytic signals were normalized with the same scale followed by the peak ratio calculation step, as shown in Eqs. 7 and 8. In the last step, the material permittivity was computed using Eqs. 9 and 10.

IV. RESULT AND DISCUSSION

The proposed method was evaluated from three perspectives. First, the analytic peak ratio was characterized when facing different GPR parameters. The analysis and characterization in this section were conducted using FDTD based numerical simulation. Second, the material permittivity was estimated by using experimental real radar data. Finally, the applicability of the method is checked by measuring the depth of the reinforced rebar inside the concrete.

A. CHARACTERISTIC OF ANALYTIC PEAK RATIO

The analytic peak ratio is designed to be used in a wide variety of GPR types and configurations. Thus, in this section, we show the characteristics of this method when facing several GPR parameters. Some parts have been briefly presented in [30].

Figure 8 shows the relationship between peak ratio and material relative permittivity with various conductivities. According to this figure, there is relatively good agreement and consistency between the proposed feature and the material relative permittivity. In addition, this correlation function is not affected by the material conductivity.

Then, according to Fig. 9(a), the correlation between analytic peak ratio and material permittivity is also not affected by the GPR pulse waveform shapes (monocycle and Ricker pulses). Figure 9(b) reveals that the waveform center frequency also does not affect the correlation unless in the lowest frequency (1 GHz) with a small change. These results

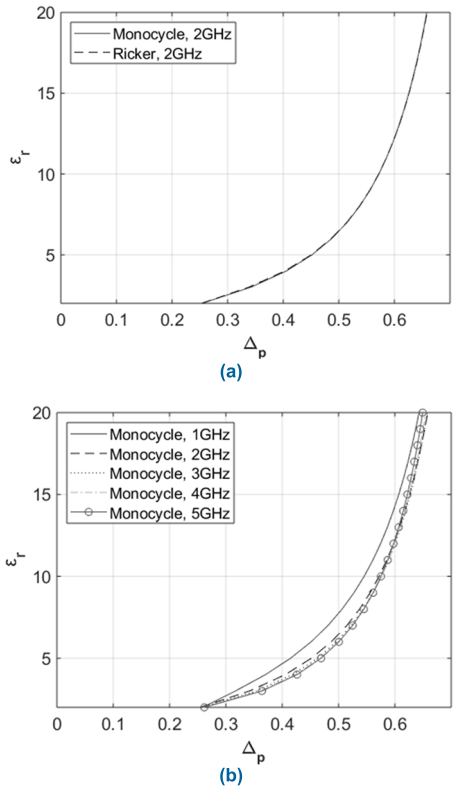

FIGURE 9. Effect of the input waveform to permittivity-analytic peak ratio relationship with change of: (a) shape and (b) center frequency.

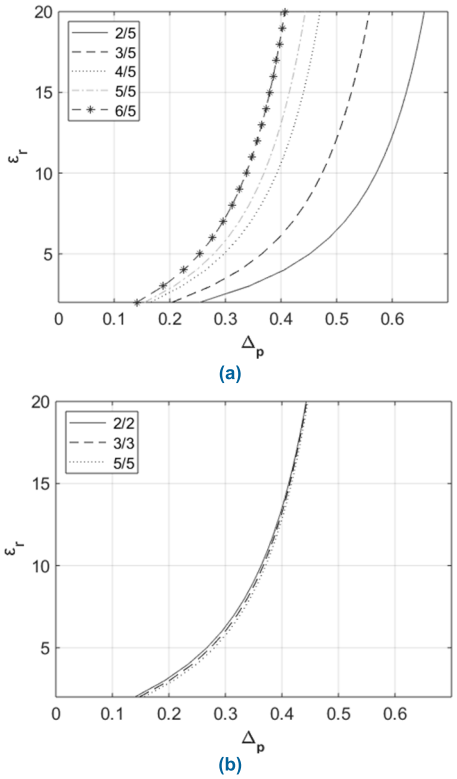

FIGURE 10. Effect of GPR configuration ratio x/y to permittivity-analytic peak ratio with: (a) different ratio, and (b) equal ratio.

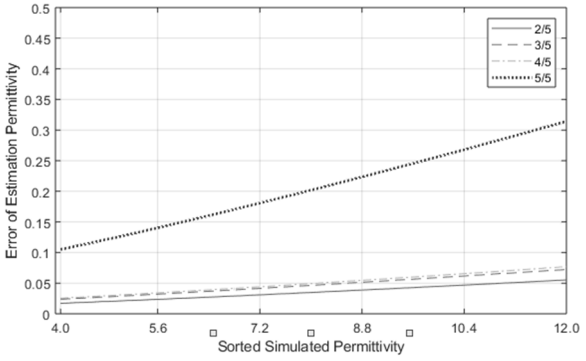

FIGURE 11. Estimation error in simulated material within different GPR configuration ratio.

confirm the adaptability of the method facing the change in GPR parameters without recalibration or during measurement, so it can be implemented for the adaptive or cognitive radar concept.

Since the proposed feature uses the direct antenna coupling signal as a reference of estimation, the correlation will be affected by the change in distance between transmitter and receiver antenna and subsequently between antenna and material surface. Thus, we consider investigating the effect of the ratio between those two distances on the correlation pattern. Figure 10 (a) shows that different configuration ratios will shift the correlation function of the peak ratio and material permittivity. A higher ratio will make the correlation sharper. However, in the case of distance change, while the ratio is fixed, the correlation ratio patterns are identical (Fig. 10(b)).

The evaluation of this method for an estimation using the interpolation technique with synthetic data is shown in Fig. 11. Fig. 11 shows us that the error of estimation increases when the relative permittivity increases due to the correlation between analytic peak ratio and relative permittivity; at high permittivity, the correlation is sharper than at low permittivity. A very sharp correlation indicates that the peak analytic ratio becomes more sensitive to the change in material permittivity. This characteristic is applied to all configuration ratios. Additionally, there is a significant error in the 5/5 ratio compared with other configurations. This is the effect of the sharpness of the characteristic curve shape of the high configuration ratio (see Fig. 10(a)). This result confirms that in a very sharp correlation, the proposed feature is more sensitive to the change in material permittivity, so the error estimation possibly increases. In short, this method is recommended for a small GPR configuration ratio.

B. MATERIAL PERMITTIVITY ESTIMATION

Using the method in Section II. C, the calculated ground truth of the tested material permittivity measured in a configuration ratio of 5/5 is shown in Table 1. The propagation time of

TABLE 1. Ground truth of material permittivity.

Material	Thickness (mm)	Δt (ns)	$\widetilde{\varepsilon_r}$
Clay Brick	64	0.718	2.83
Concrete Brick	60	0.846	4.47
Concrete Slab	60	0.923	5.33

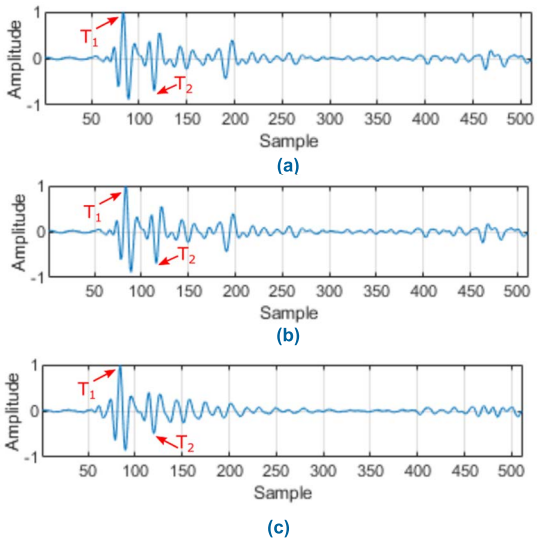

FIGURE 12. Radar signal for computing the ground truth of permittivity: (a) clay brick, (b) concrete brick, and (c) concrete slab.

TABLE 2. Calculation of shift factor using concrete brick.

Configuration Ratio (x/y)	$\widetilde{\varepsilon_r}$	F
3/5	4.47	0.366
4/5		0.316
5/5		0.239

each tested material is shown in Fig. 12. Then, to calibrate this shift factor value, we used the concrete brick as a reference. Table 2 shows the obtained average shift factor using 100 measurements to connect the simulation and experimental data (see Eq. 8).

By applying the proposed method, we estimate two materials: clay brick and concrete slab. The results of the estimation and comparative analysis are shown in Table 3. The results were obtained using 100 measured data points in each configuration range and materials. According to this table, the method can estimate the permittivity with acceptable accuracy. The precision of the estimation is confirmed by a relatively small standard deviation in all configuration ratios. From the mean value in each configuration range, the highest estimation errors for clay brick and concrete slabs are approximately 0.32 and 0.53, respectively. The smallest estimation errors are 0.08 and 0.06 for both materials, respectively. The average estimation for all configuration ranges has a small difference from the actual values for both materials.

TABLE 3. Result of estimation of clay brick and concrete slab.

Clay Brick			
Radar-Object Range (cm)	Ground truth	Estimated Permittivity	
		Mean	Standard Deviation
6	2.83	2.97	0.019
7		2.75	0.057
8		2.51	0.019
9		2.54	0.024
10		3.00	0.030
Average		**2.75**	**0.030**

Concrete Slab			
Radar-Object Range (cm)	Ground truth	Estimated Permittivity	
		Mean	Standard Deviation
6	5.33	5.77	0.047
7		5.27	0.041
8		5.86	0.067
9		5.60	0.111
10		5.69	0.069
Average		**5.64**	**0.066**

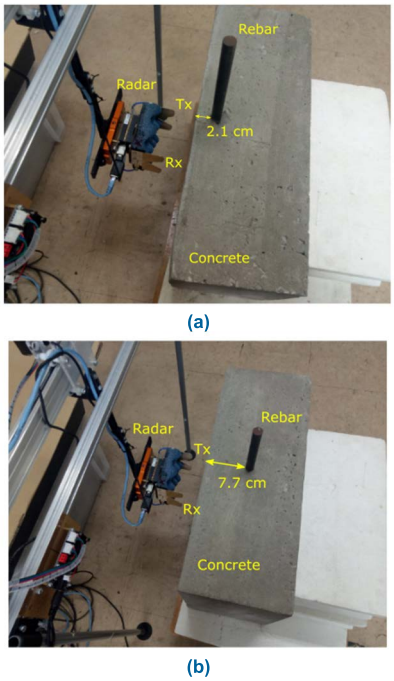

FIGURE 13. Experiment setup for rebar depth estimation on reinforced concrete with depth of: (a) 2.1 cm (concrete A), and (b) 7.7 cm (concrete B).

The material permittivity estimation using surface reflection has a limitation depending on the stability of the radar amplitude, as mentioned in [15]. The variation in the error of each configuration ratio in this study confirms this approach limitation. A nonuniform and rough shape of the clay brick also makes the estimation less accurate.

For ranges of 7 cm and 9 cm, the method employs one and two interpolations for two different cases (Eq. 10). The result in those cases confirms the applicability of both

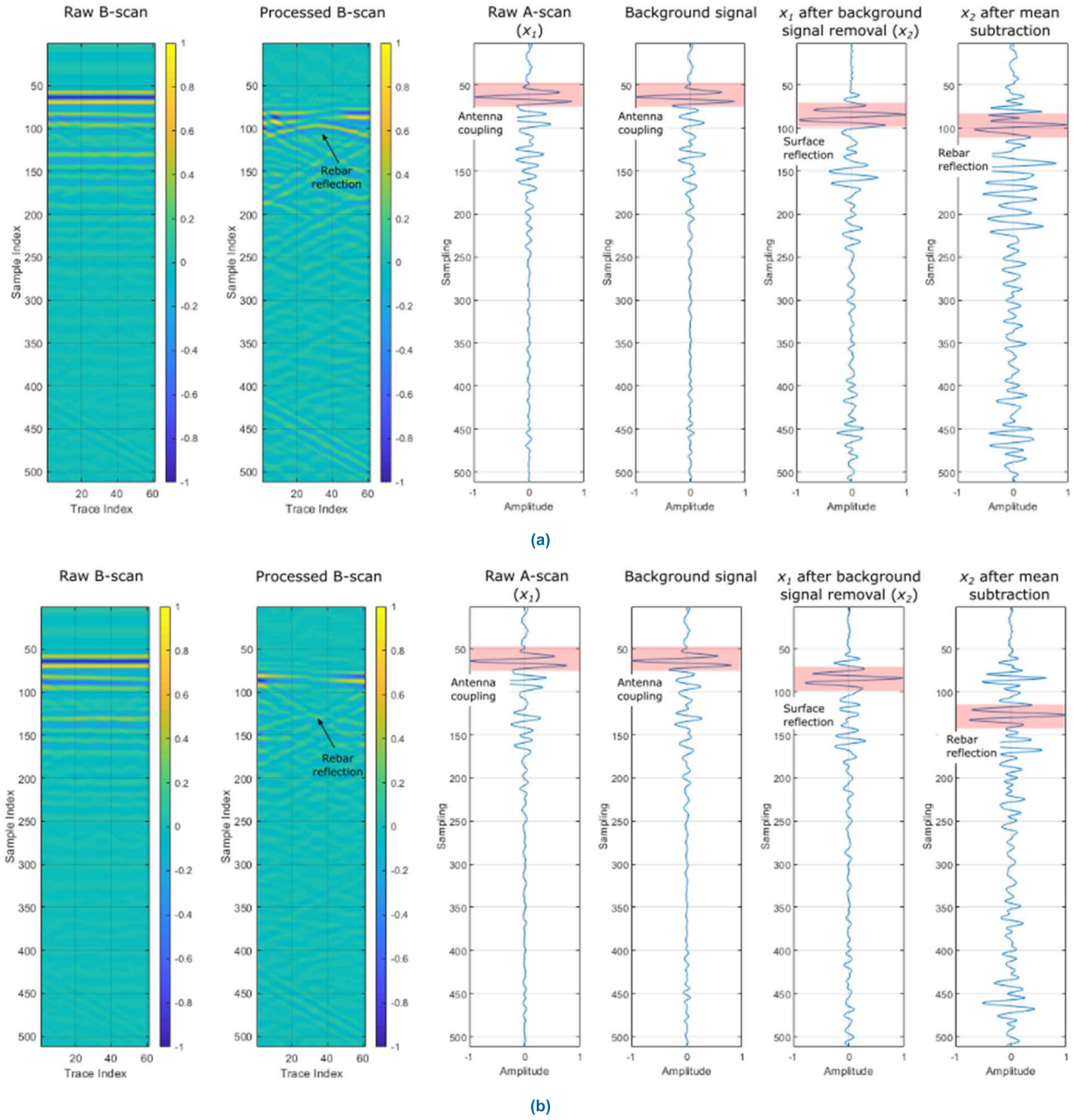

FIGURE 14. Signal processing step to estimate the rebar depth of: (a) 2.1 cm (concrete A), and (b) 7.7 cm (concrete B).

one-interpolation (ranges of 6 cm, 8 cm, and 10 cm) and two-interpolation (ranges of 7 cm and 10 cm) methods. The performance and accuracy consistency of the method against the change in range between antenna and material under test reveals that the method is applicable by using an unstable platform such as unmanned ground or air vehicle-based radar systems.

C. ESTIMATION OF REBAR DEPTH INSIDE CONCRETE

To further evaluate the applicability of this method, we apply it to estimate the rebar depth inside the reinforced concrete. The dimension of the concrete is 50 cm × 30 cm × 17 cm. Metal rebar 1.5 cm in diameter is embedded inside the concrete at depths of approximately 2.1 cm (concrete A) and 7.7 cm (concrete B). The range of the radar material is 10 cm, or the configuration ratio is 10/10. The B-scan data are recorded by 61 traces with 5 mm steps. The experimental setup to conduct this study for both concretes is shown in Fig. 13.

By estimating the permittivity and analyzing the time delay of rebar reflection, we obtained the depth of the rebar by computing Eq. (12). Since it is difficult to see the rebar

TABLE 4. Estimation of the reinforced concrete rebar depth.

Concrete	Rebar Depth (cm)	Estimated Permittivity	Time to rebar (ns)	Estimated Rebar depth (cm)
A	2.1	4.68	0.308	2.13
B	7.7	4.68	1.103	7.65

reflection from A-scan data, we employ B-scan data and process it to extract the signal components: surface and rebar reflections. The process contains DC-shift removal, bandpass filtering following the antenna bandwidth, background signal removal (to extract the surface reflection timing), and mean subtraction (to remove the surface reflection and extract the rebar reflection timing). The background signal is the radar data measured without object which means that the recorded signal consists of antenna coupling and background noise only. The processing results (both B-scan and A-scan at trace-31 (x_1)) are shown in Fig. 14. From those figures, using the aforementioned signal processing methods, we can extract the delay time of rebar reflections even when the rebar is embedded. The concrete permittivity and rebar depth estimation results are shown in Table 4. Examining the table, we can see the estimation of the permittivity of concrete, delay time, and rebar depth. The estimation using the proposed method is relatively accurate compared with the actual depth.

Those two different depth cases confidently confirm the proposed method works in different situation. In a more complex case such as several rebars embedded in a concrete specimen, the reflection signal will be more complex. In this such situation, an advanced signal enhancement method is required aiming an accurate delay time estimation.

V. CONCLUSION

This paper proposes a new and practicable method to determine the material permittivity using air-coupled GPR. The method employs the ratio of the analytic representation signal between antenna direct coupling and material surface reflection. The antenna direct coupling component in this study is exploited as a reference of the ratio, since this signal commonly exists with no modification, and the value is relatively constant. Both numerical simulations and experiments demonstrate that the method can estimate material permittivity with considerable accuracy. In addition, the experimental results show the ability to accurately estimate the rebar depth inside reinforced concrete.

Because the method can adapt in the range between antenna and material, it is promising for application in mobile platforms such as unmanned aerial- or ground-based GPR, which is currently massively explored. In addition, the consistency of the method against the waveform and center frequency during measurement without recalibration makes it feasible to apply the method to the possible future cognitive radar concept, which can improve the radar performance.

However, this method has some limitations as follows. First, this method works well specifically on materials with a relatively flat surface. A very rough surface will decrease the accuracy, since this will scatter the electromagnetic wave. Thus, the proposed method is appropriate for relatively flat materials such as reinforced concrete, walls, and other building materials. In addition, this method assumes that the material permittivity is vertically constant along the materials. The method can be applied for heterogeneous materials, but the method holds that assumption. In other words, the method can only estimate the horizontal variation of permittivity of near-surface material. Another assumption that the permittivity of a material is constant for all radar frequency components must also be held.

ACKNOWLEDGMENT

The authors would like to thank the anonymous reviewers for their insightful comments and suggestions.

REFERENCES

[1] H. M. Jol, *Ground Penetrating Radar Theory and Applications*. Amsterdam, The Netherlands: Elsevier, 2008.

[2] A. Benedetto and L. Pajewski, Eds., *Civil Engineering Applications of Ground Penetrating Radar*. Cham, Switzerland: Springer, 2015.

[3] F. Soldovieri, R. Solimene, L. L. Monte, M. Bavusi, and A. Loperte, "Sparse reconstruction from GPR data with applications to Rebar detection," *IEEE Trans. Instrum. Meas.*, vol. 60, no. 3, pp. 1070–1079, Mar. 2011.

[4] R. Solimene, G. Leone, and A. D. Aversano, "MUSIC algorithms for rebar detection," *J. Geophys. Eng.*, vol. 10, no. 6, 2013, Art. no. 064006.

[5] N. J. Cassidy, R. Eddies, and S. Dods, "Void detection beneath reinforced concrete sections: The practical application of ground-penetrating radar and ultrasonic techniques," *J. Appl. Geophys.*, vol. 74, no. 4, pp. 263–276, Aug. 2011.

[6] H. Li, N. Li, R. Wu, H. Wang, Z. Gui, and D. Song, "GPR-RCNN: An algorithm of subsurface defect detection for airport runway based on GPR," *IEEE Robot. Autom. Lett.*, vol. 6, no. 2, pp. 3001–3008, Apr. 2021.

[7] G. Roqueta, L. Jofre, and M. Q. Feng, "Analysis of the electromagnetic signature of reinforced concrete structures for nondestructive evaluation of corrosion damage," *IEEE Trans. Instrum. Meas.*, vol. 61, no. 4, pp. 1090–1098, Apr. 2012.

[8] S. Laurens, "Non-destructive evaluation of concrete moisture by GPR: Experimental study and direct modeling," *Mater. Struct.*, vol. 38, no. 283, pp. 827–832, Nov. 2005.

[9] M. Nishimoto, B. P. A. Rohman, and Y. Naka, "Analysis of H-polarized wave scattering by a metal cylinder covered with inhomogeneous material," in *Proc. Int. Symp. Antennas Propag. (ISAP)*, Busan, south Korea, Oct. 2018, pp. 1–2.

[10] Z. M. Sbartaï, S. Laurens, J.-P. Balayssac, G. Arliguie, and G. Ballivy, "Ability of the direct wave of radar ground-coupled antenna for NDT of concrete structures," *NDT E Int.*, vol. 39, no. 5, pp. 400–407, Jul. 2006.

[11] D. Comite, A. Galli, S. E. Lauro, E. Mattei, and E. Pettinelli, "Analysis of GPR early-time signal features for the evaluation of soil permittivity through numerical and experimental surveys," *IEEE J. Sel. Topics Appl. Earth Observ. Remote Sens.*, vol. 9, no. 1, pp. 178–187, Jan. 2016.

[12] A. Di Matteo, E. Pettinelli, and E. Slob, "Early-time GPR signal attributes to estimate soil dielectric permittivity: A theoretical study," *IEEE Trans. Geosci. Remote Sens.*, vol. 51, no. 3, pp. 1643–1654, Mar. 2013.

[13] E. Pettinelli, A. Di Matteo, S. E. Beaubien, E. Mattei, S. E. Lauro, A. Galli, and G. Vannaroni, "A controlled experiment to investigate the correlation between early-time signal attributes of ground-coupled radar and soil dielectric properties," *J. Appl. Geophys.*, vol. 101, pp. 68–76, Feb. 2014.

[14] G. Hislop, "Permittivity estimation using coupling of commercial ground penetrating radars," *IEEE Trans. Geosci. Remote Sens.*, vol. 53, no. 8, pp. 4157–4164, Aug. 2015.

[15] X. Liu, J. Chen, X. Cui, Q. Liu, X. Cao, and X. Chen, "Measurement of soil water content using ground-penetrating radar: A review of current methods," *Int. J. Digit. Earth*, vol. 12, no. 1, pp. 95–118, Jan. 2019.

[16] K. Wu, G. A. Rodriguez, M. Zajc, E. Jacquemin, M. Clément, A. De Coster, and S. Lambot, "A new drone-borne GPR for soil moisture mapping," *Remote Sens. Environ.*, vol. 235, Dec. 2019, Art. no. 111456.
[17] J. Colorado, M. Perez, I. Mondragon, D. Mendez, C. Parra, C. Devia, J. Martinez-Moritz, and L. Neira, "An integrated aerial system for landmine detection: SDR-based ground penetrating radar onboard an autonomous drone," *Adv. Robot.*, vol. 31, no. 15, pp. 791–808, Aug. 2017.
[18] B. P. A. Rohman, M. B. Andra, H. F. Putra, D. H. Fandiantoro, and M. Nishimoto, "Multisensory surveillance drone for survivor detection and geolocalization in complex post-disaster environment," in *Proc. IEEE Int. Geosci. Remote Sens. Symp. (IGARSS)*, Yokohama, Japan, Jul. 2019, pp. 9368–9371.
[19] S. Laurens, "Influence of concrete relative humidity on the amplitude of ground-penetrating radar (GPR) signal," *Mater. Struct.*, vol. 35, no. 248, pp. 198–203, May 2002.
[20] G. Serbin and D. Or, "Ground-penetrating radar measurement of soil water content dynamics using a suspended horn antenna," *IEEE Trans. Geosci. Remote Sens.*, vol. 42, no. 8, pp. 1695–1705, Aug. 2004.
[21] M. Aftanas, J. Sachs, M. Drutarovský, and D. Kocur, "Efficient and fast method of wall parameter estimation by using UWB radar system," *Frequenz*, vol. 63, nos. 11–12, pp. 231–235, 2009.
[22] R. Linnehan, J. Schindler, D. Brady, R. Kozma, R. Deming, and L. Perlovsky, "Dynamic logic applied to SAR data for parameter estimation behind walls," in *Proc. IEEE Radar Conf.*, Apr. 2007, pp. 850–855.
[23] S. Sadeghi, K. Mohammadpour-Aghdam, K. Ren, R. Faraji-Dana, and R. J. Burkholder, "A pole-extraction algorithm for wall characterization in through-the-wall imaging systems," *IEEE Trans. Antennas Propag.*, vol. 67, no. 11, pp. 7106–7113, Nov. 2019.
[24] Z. Leng and I. L. Al-Qadi, "An innovative method for measuring pavement dielectric constant using the extended CMP method with two air-coupled GPR systems," *NDT E Int.*, vol. 66, pp. 90–98, Sep. 2014.
[25] V. Marecos, S. Fontul, M. Solla, and M. D. L. Antunes, "Evaluation of the feasibility of common mid-point approach for air-coupled GPR applied to road pavement assessment," *Measurement*, vol. 128, pp. 295–305, Nov. 2018.
[26] S. Lambot, E. C. Slob, and I. Van Den Bosch, "Estimating soil electric properties from monostatic ground-penetrating radar signal inversion in the frequency domain," *Water Resour. Res.*, vol. 40, no. 4, pp. 1–12, 2004.
[27] S. Lambot, L. Weihermüller, and J. A. Huisman, "Analysis of air-launched ground-penetrating radar techniques to measure the soil surface water content," *Water Resour. Res.*, vol. 42, no. 11, pp. 2–12, 2006.
[28] M. L. Manna, P. Monsurro, P. Tommasino, and A. Trifiletti, "Adaptive spectrum controlled waveforms for cognitive radar," in *Proc. IEEE Radar Conf. (RadarConf)*, May 2016, pp. 1–4, doi: 10.1109/RADAR.2016.7485120.
[29] S. Haykin, Y. Xue, and T. N. Davidson, "Optimal waveform design for cognitive radar," in *Proc. 42nd Asilomar Conf. Signals, Syst. Comput.*, Oct. 2008, pp. 3–7.
[30] B. P. A. Rohman and M. Nishimoto, "Concrete dielectric constant estimation based on analytic signal peak ratio of GPR response for non-destructive inspection," in *Proc. IEEE Int. Geosci. Remote Sens. Symp. (IGARSS)*, Yokohama, Japan, Jul. 2019, pp. 6376–6379.
[31] C. Warren, A. Giannopoulos, and I. Giannakis, "gprMax: Open source software to simulate electromagnetic wave propagation for ground penetrating radar," *Comput. Phys. Commun.*, vol. 209, pp. 163–170, Dec. 2016.

BUDIMAN P. A. ROHMAN (Member, IEEE) received the B.E. degree in engineering physics from the Sepuluh Nopember Institute of Technology, Surabaya, Indonesia, in 2009, and the M.E. degree in computer science and electrical engineering and the Ph.D. degree in human and environmental informatics from Kumamoto University, Japan, in 2018 and 2021, respectively. Since 2015, he has been with the Research Center for Electronics and Telecommunication, National Research and Innovation Agency, Indonesia. In 2020, he was a Visiting Researcher with the Fraunhofer Institute for High-Frequency Physics and Radar Techniques FHR, Wachtberg, Germany. Currently, he is a Researcher with Kumamoto University. His research interests include signal processing, radar signal processing and imaging, machine learning, and embedded systems.

MASAHIKO NISHIMOTO (Member, IEEE) received the B.E. degree in electronic engineering from Kumamoto University, Japan, in 1982, and the M.E. and D.E. degrees in computer science and communication engineering from Kyushu University, Fukuoka, Japan, in 1984 and 1987, respectively. Since 1987, he has been with the Department of Electrical Engineering and Computer Science, Kumamoto University. From 2001 to 2002, he was a Visiting Scholar at Duke University, Durham, NC, USA. He is currently a Professor with the Faculty of Advanced Science and Technology, Kumamoto University. His research interests include radar signal processing, application of ground penetrating radar, scattering and diffraction of electromagnetic waves, and computational electromagnetics. From 2009 to 2010, he served as IEEE AP-S Fukuoka Chapter Chair. From 2011 to 2013, he served as the Chair for the Technical Committee on Electromagnetic Theory in Electronics Society, IEICE.

KOHICHI OGATA (Member, IEEE) was born in Kumamoto, Japan, in 1967. He received the B.E., M.E., and Ph.D. degrees in engineering from Kumamoto University, Kumamoto, in 1989, 1991, and 1994, respectively. He is currently an Associate Professor with the Department of Computer Science and Electrical Engineering, Faculty of Advanced Science and Technology, Kumamoto University. His research interests include signal processing, speech processing, and image processing, such as measurement of speech production process and development of its applications, development of eye-gaze interface systems, and augmented reality application systems.